# Design and Experiments of a Dragonfly-Inspired Robot

Christopher DiLeo and Xinyan Deng*

*Department of Mechanical Engineering, University of Delaware, Newark, DE - USA*

*deng@udel.edu

**Abstract**

This paper describes the design of dragonfly-inspired robots. Dragonflies demonstrate unique and superior flight performances than most of the other insect species. They are equipped with two pairs of independently controlled wings. The high level of dexterity in wing motion of the dragonfly allows it to hover, fly fast forward, make turns rapidly, fly sideways, and even glide. A dragonfly-inspired robot which could effectively mimic those kinematics would potentially exhibit superior flight performance than existing designs of insect robots. In this paper, we introduce two generations of robotic dragonfly prototypes developed to implement simplified dragonfly kinematics. Preliminary experiments on kinematics and aerodynamic force measurements of the prototypes are also presented.

*keywords*: Flapping flight, Micro aerial vehicles, Dragonfly Robots, Biologically Inspired Robots, Biomimetics.

## 1 INTRODUCTION

Dragonfly is one of the oldest and most maneuverable flying insects on earth. Their flight performance far exceeds many other flying insect species. They can hover, cruise up to 54km/h, turn 180 in three wing beats, fly sideways, glide, and even fly backwards [1] [2]. They intercept prey in air with amazing speed and accuracy. Dragonfly has inspired engineers to build four-winged micro aerial vehicles, for example, the Wowwee dragonfly robot [3] and Delfly [4]. These dragonfly MAVs share the same feature of a coupled four-wing mechanism based on two-wing structures. In their design, the leading edges of the principle wing pair are extended to form the leading edge of the second pair, and as a result all four wings flap on the same stroke plane and there is no distinction between the forewing and hindwings.

In this study, we aim to build a dragonfly insect robot equipped with two separate pairs of wings. As observed in nature, dragonflies control their forewing and hindwings independently by their powerful and complicated thorax muscles. As a result, the two pairs of wings employ different wing kinematics and relative phase angles during different flight modes. The advantages of two separate pairs of wings are not only reflected in the increased total aerodynamic lift over one pair of wings, but also increased flight control inputs and stabilization techniques in different flight modes.

Biological locomotory systems are typically quite complex, and do not lend themselves directly to analytical methods when attempting to understand the physical phenomena at hand. A properly designed experimental

testbed can facilitate the study of a wide range of natural phenomena. We have developed a pair of dragonfly flappers to reproduce the wing kinematics of dragonflies in hover and forward flight, while measuring the instantaneous aerodynamic forces and visualizing the flow field. The flapper allows for the testing of high stroke plane kinematics as seen in dragonflies and can closely mimic the real dragonfly wing motion, a capability lacking in the very few experimental setup so far [5] [6]. Once the information garnered from these experiments has been utilized in a robotic prototype design, the testbed can also be used to evaluate the implementation of the robotic dragonflies.

Two generations of robotic dragonfly prototypes have been constructed, utilizing different manufacturing techniques. The prototypes take inspiration from the efficiency in hovering flight of dragonflies. The natural kinematics of a dragonfly have been altered for simplicity of mechanical design, in an effort to reduce the weight of the prototype and maximize lift force. The design process for each prototype is explained in detail, as well as experimental measurements on kinematics and aerodynamics.

# 2 Dragonfly Flight

Dragonflies have survived millions of years of evolution and are one of the most stable and maneuverable flyers in nature. They are also one of the very few species which can capture preys in air. Their horizontal body posture allows them to change flight modes from hovering to fast forward or turning swiftly and follow a target closely. Unlike most other insects, dragonflies can also fly backwards, sideways and even glide. Their flight speed is as high as 90km/h, and acceleration is as high as 130m/$s^2$. The maximum thrust force their wings generate can go up to thirteen times their body weight. Videos of dragonfly flight also show dragonflies turn 180 degrees in only three wingbeats. In general, the wingbeat frequency of dragonfly ranges from 20-90 Hz.

The flight kinematics of a dragonfly differ significantly from most insects in that they have two pairs of independently-controllable wings. The high level of dexterity in wing motion of the dragonfly allows for its excellent maneuverability, and a robot which could effectively mimic those kinematics would potentially exhibit superior flight performance than existing designs.

## 2.1 Wing Kinematics

Dragonfly flight kinematics have been studied extensively from a biological perspective [7], [8], [9], [10], [11], [12], [13], [14], [15], [16]. Experiments and measurements on the flight kinematics of different species of dragonflies are available [17], [18], [19], [20], [21]. It has been observed that while hovering, dragonfly wing motion is mostly confined to the stroke plane, which is defined in Figure 1.

Figure 1 shows the wing coordinate system, where $\beta$ is the stroke plane angle with respect to the vertical. $\alpha$ is the wing stroke amplitude within the stroke plane. $\psi$ is the angle of attack w.r.t the stroke plane. Deviation angle defines the angle deviated from the stroke plane. The Reynolds number range includes all flight conditions such as hovering and forward flight. Table 1 shows the range of dragonfly wing kinematics based on biological studies [10], [22].

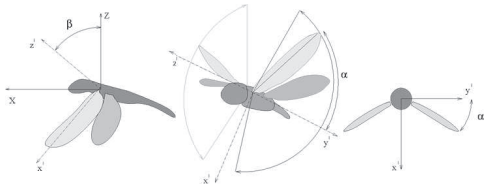

Figure 1: Wing Coordinate System: the stroke plane is defined as the x'y' plane. The stroke plane angle is $\beta$. $\alpha$ is the amplitude within the stroke plane.

| $\beta$ | $\alpha$ | $\psi$ | deviation | Re |
|---|---|---|---|---|
| -5 to 90 | -90 to 90 | -30 to 60 | -20 to 20 | 50 to $10^4$ |

Table 1: Range of Wing Motion Kinematics for Dragonfly

It has been found that the phase difference between the forewings and hindwings of dragonfly changes as flight condition varies [23]. During hovering, dragonflies employ out-of-phase counter-stroking of the forewing and hindwing, mostly due to stability and vibration suppression purposes. During forward flight, they employ phase difference between 60-90 degrees. Using a pair of horizontally stacked robotic wings, researchers found that the wing-wing interactions in dragonfly may be advantageous for power efficiency purposes [6]. Although in the aforementioned study, the motion is close to hoverflies and damselflies, which primarily flap in a horizontal stroke plane and use smaller phase shifts.

The high level of control that dragonflies exert over their wings can be traced to the way the flight muscles on the wing base. The flapping motion of the wings is controlled by separate muscles than those which control feathering motion, in contrast to most other flying insects, in which muscles that are responsible for flapping also control feathering [24].

## 2.2 Aerodynamic Characteristics

Since dragonflies flap in a close to vertical stroke plane for hovering, most of the lift generation is caused by pressure drag on the downstroke. The wing acts like an oar dragging through the water; the drag force on the wing is directed upwards while the wing is pushing down. This flapping regime has the benefit of lowering the specific power required for flapping by minimizing the force on the wing for the upstroke. For normal (horizontal stroke plane) hovering, the drag is a parasitic force: it does not contribute to the vertical force, and therefore should be minimized. The contribution of drag forces to net vertical force is explored and analyzed by computational fluid methods in [15].

Unsteady aerodynamic mechanisms have been found in insect flight [25]. The introduction of quasi-steady analytical models into the aerodynamics of insect flight has seen much progress over the past decade. The extent to which these unsteady terms are applicable to dragonfly kinematics has yet to be determined since dragonflies assume different wing kinematics, especially the high stroke plane angle resulted drag based lift. While some of the unsteady phenomena are markedly absent for dragonflies (most obviously clap-and-fling), others probably

play a role in lift generation such as wing-wing interactions [10] [26].

### 2.3 Wing Flexibility and Passive Rotation

Passive rotation is generally a mechanism which allows the wing to rotate without using active control, this feature is present in most insects rather than bats, birds or other larger flying animals. Dragonfly wings have the flexibility to rotate and change their effective angle of attack without actively using muscles to perform this task. It has been found that both fluid forces [27], and the wing's own inertial forces [28] facilitate this rotation.

Dragonfly wings have an inherent flexibility which allows the wing to deform during flight. Dragonfly wings exhibit a torsional deformation from root to tip (similar to helicopter blades). This balances the effective angle of attack along the length of the wing. The deformation of the wing is also aided by its own inertial forces. The center of mass of a dragonfly wing is behind its rotational axis, which forces the wing to rotate during stroke reversal. The inertial force exerted on the wing is controlled by the size of the pterostigma, a heavy spot near the tip of the wing that affects the wings rotational inertia [29]. The actual rotation of the wing must be the result of *some* active torsional force though, since the timing of the rotation within the stroke cycle is too early to be entirely supplied by the inertial forces. More recently, it has been suggested that the fluid forces do supply the majority of the rotation [27]. In this work, we will also incorporate passive rotation of the wing into the robot design.

## 3 Dragonfly Robot Design and Experimental Apparatus

The goal of this project was to design a dragonfly robot capable of hovering flight. We have developed two generations of robotic prototypes. Both pairs of wings are driven by one motor to achieve the power stroke flapping motion, while a tunable phase difference between the forewings and hindwings was achieved by a variable length coupler link. Flapping alone will not generate any net lift, therefore passive rotation of the wings were incorporated into the design to generate angle of attack. The design of one motor driving both wings results from the consideration of weight and simplification purposes.

### 3.1 Experimental Apparatus to study dragonfly aerodynamics

In order to properly test flapping kinematics, we developed an experimental apparatus to reproduce a wide range of actual dragonfly kinematics, in particular, to realize the high stroke plane motion of actual dragonflies. Compared to previous flapping mechanisms [30], [9], [31], [6], [16], [10], the two main improvements of the current dragonfly flappers are the ability to place the base of two wings very close together to capture the fluid interactions, and the ability to test kinematics which incorporated a high stroke-plane angle in both hovering and forward flight cases. Details of the flapper mechanism can be found in [32]. Figure 2 shows the experimental apparatus.

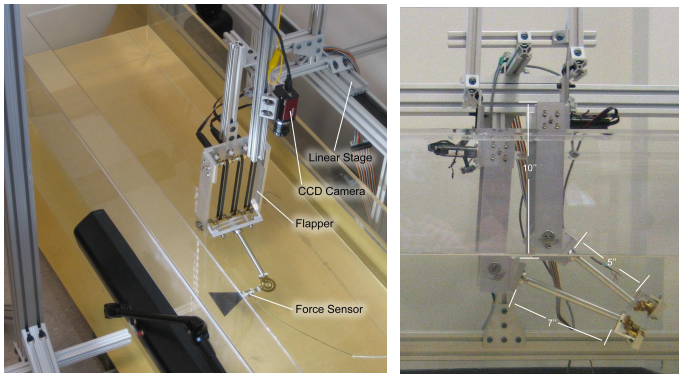


(a) Bird's eye view of flapper (b) Side view of two flappers

Figure 2: Experimental Setup

## 3.2 DC Motor Driven Double Slider-Crank Mechanism

The mechanical drive for the prototype is a double slider-crank mechanism. The slider crank mechanism transmits the rotational motion of the motor to the wings, which exhibit a flapping motion. This design has the advantage of creating a perfectly symmetric wing motion. The slider-crank has three functional parts: the crank, the connecting rod and the slider. The crank (in this case, a gear) is constrained so it may rotate in a complete circle. The connecting rod (a carbon fiber linkage) is pinned at both ends: one to the gear and one to the slider. The slider is constrained to linear motion along a post. As the gear, driven by the motor, rotates, its motion is transmitted through the linkage to the slider, which moves linearly on the post. This can be seen in Figures 3 and 4, where the motion of the gear (labeled '1') drives the motion of the slider (labeled '2'). There is a dedicated slider for both the fore- and hind-wings (Figure 5(b)). The phase link joint allows one gear to serve as the crank for both sliders, and is presented in the next section.

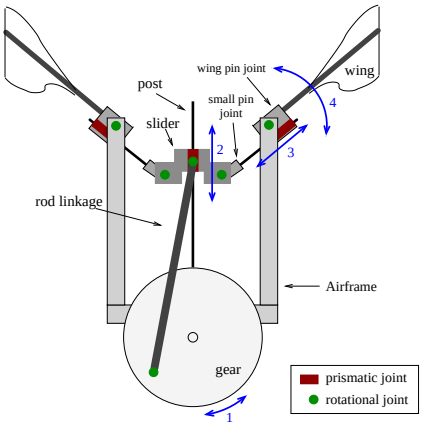


Figure 3: Schematic of slider mechanism: showing constraints on individual component's motion. Numbered arrows show progression of prescribed motion from gear to wing

The slider crank is in charge of realizing the linear motion of the slider. Once this has been accomplished, the flapping motion of the wing must be realized. This is done by utilizing two pin joints, whose interactions

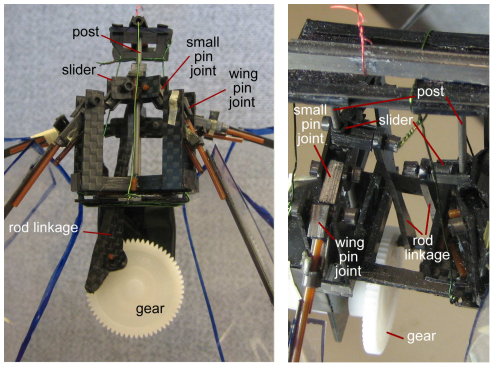


(a) Front View (b) Bird's Eye View

Figure 4: Photos of double slider crank mechanism

transform the linear motion to a flapping motion. A small pin joint is attached to the slider. The small pin joint consists of two carbon fiber tubes: one to support the pin which attaches it to the slider, and one to house a garolite rod, which slides through the wing pin joint (see Figure 5(a)). This sliding motion of the rod is labeled '3' in Figure 3. As the slider moves on the post, the rod keeps the small pin joint aligned with the wing pin joint, whose position is fixed w.r.t the airframe. Thus, the up and down motion of the slider becomes an angular rocking motion of the small pin joint, which is transmitted through the wing pin joint to the wing (labeled '4'). The mechanism functions such that the axis of the garolite rod (on the small pin joint) is always parallel to the axis of the wing spar. The wing pin joint is attached to the wing spar, and as the pin joint rotates, so does the wing; rotation of the pin joint is prescribed as the flapping motion of the wing.

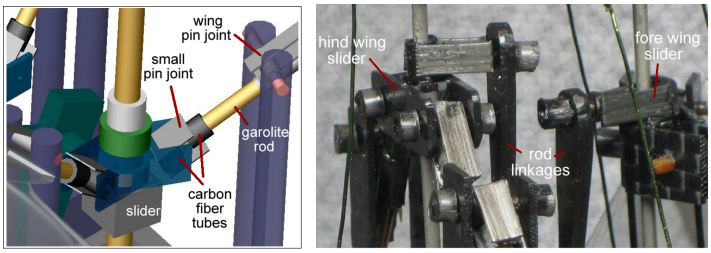


(a) Solidworks model of the slider and pin joints (b) View of fore- and hind-wing sliders

Figure 5: Solidworks model of slider and pin joints and photos of the structure

## 3.3 Variable Phase Angle Between Forewings and Hindwings

In dragonfly flight, the phase difference between the forewing and hindwing plays an important role in force generation [31] [6]. In our mechanism, the amplitude of each pair of wing can be varied, as can the phase difference. Both of these kinematic parameters can be adjusted on the prototype with the phase link joint, shown in Figure 7.

The phase difference can be changed by increasing the length of the phase link, and relative amplitude can be changed by rotating the phase link. Figure 8(a) shows the side view and front view of the gear mechanism design.

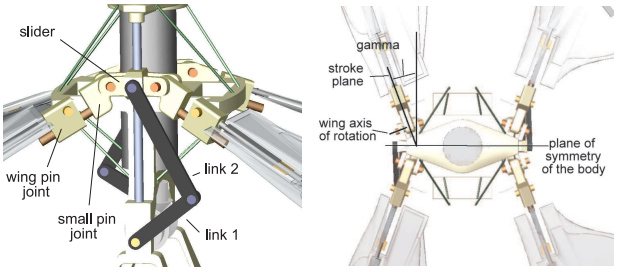


(a) Slider Mechanism (b) Top down view

Figure 6: (a)Double Slider-Crank mechanism. Notice that link 1 replaces the gear shown in Figure 7. (b)Top view of prototype illustrating stroke plane deviation.

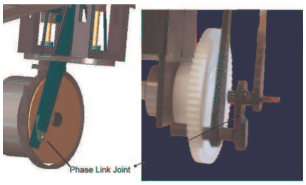


Figure 7: Phase link joint (light green). Defines the phase difference between rod linkages (in dark green) which drive the sliders for fore and hind wings. The actual phase link joint is also shown on the prototype.

The phase link effectively moves the attachment point of the forewing rod linkage on the gear (point 2 in Figure 8(b)), thus moving it forward or backward in its cycle with respect to the hindwing (point 1). The link length (l) needed for a given phase shift, $\psi$ is calculated as,

$$l^2 = r_1^2 + r_2^2 - 2r_1 r_2 \cos\psi \tag{1}$$

where $r_1$ and $r_2$ are the effective radii of the hind- and forewings, respectively. This radius is used in equations 2 and 3 to calculate the amplitude of the wing's rotation.

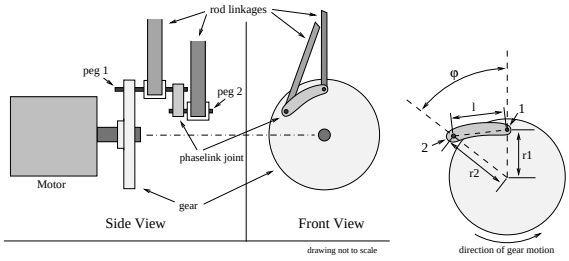


(a) Gear mechanism (first generation) (b) Coupler link

Figure 8: Gear mechanism and phase difference coupler link for the first generation robot

### 3.4 Wing Passive Rotation Joint

Passive rotation exists in most insect wings during flight [27] [28]. In our design, passive rotation was achieved in the mechanism by allowing the wing to rotate freely within a constrained variable space. The wing is allowed to rotate 90 degrees from a horizontal position, to a vertical position. In practice, the wing can achieve effective angles slightly outside this range due to wing flexibility and component tolerances (this is illustrated in the measured wing kinematics shown in figure 14(a). With the wing free to rotate, the actual angle of attack is determined by the aerodynamic torque, inertia, etc. During the downstroke the aerodynamic force causes a moment around the wing which holds it in a horizontal position. This maximizes the drag on the wing, which is desired because it results in an upward force on the body. During the upstroke, the aerodynamic force causes a moment around the wing which rotates it to the vertical position, which minimizes drag, and thus the downward force on the body. In the transition areas between the two strokes, the wing rotates due to a combination of aerodynamic, gravitational and inertial forces.

Figure 9(a) shows the Solidworks model for the passive rotation joint which was eventually constructed out of carbon fiber. To fulfill its function as the output link for the wing pin joint, it has two carbon fiber tubes. One houses the pin for the wing pin joint, and one serves as a sliding joint for the rod attached to the output link of the small pin joint. Figure 9(b) shows the actual wing with embedded passive rotation joint in the second generation prototype. A short garolite rod serves as the spar for the wing, to attach it to the wing pin joint. This rod is glued part-way inside a carbon fiber tube, which in turn is glued to a long carbon fiber beam. The polyester film of the wing is supported by a long carbon fiber beam, which is glued to the garolite rod that extends into the passive rotation joint. The film is also glued at another point on the garolite rod, this time in the interior of the passive rotation joint, through a gap in the joint. The two opposing carbon fiber beams restrict the rotation of the rod, as the wing will come into contact with the beams, halting its rotation.

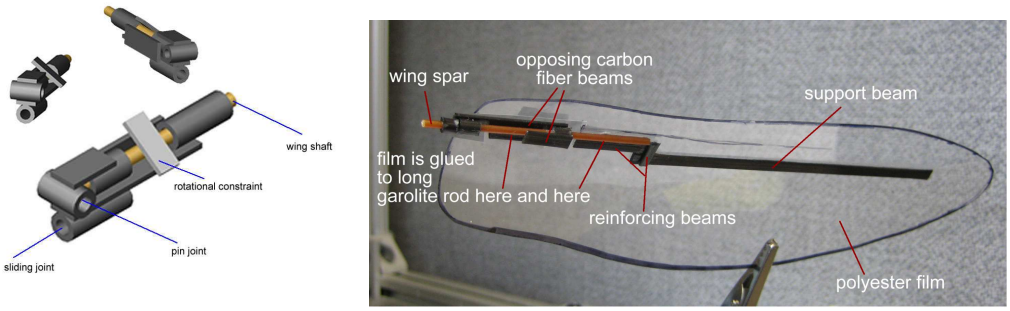


(a) Passive Rotation Joint

(b) Assembled Wing

Figure 9: Wing with passive rotation joint built out of carbon fiber and garolite.

### 3.5 Stroke Plane Angle

The stroke plane is the plane which contains the wing spar's motion (the plane in which the wing flaps.) It is always vertical ($\beta$ is $90^o$) , but the angle that it makes with the plane of symmetry of the body ($\gamma$ in Figure 6(b))

affects the adjacent wing's fluid interaction. Both the fore-and hind-wings have a $\gamma$ leaning 20 degrees away from the perpendicular. This allows for the base of the wings to be placed closer together (without shrinking the wing size) and more closely mimics an actual dragonfly's hovering stroke planes.

## 3.6 Prototype Development

The airframe and most other components of the first generation prototype were made of carbon fibers and machined in the lab. To further minimize the size of the airframe, the second-generation prototype was designed in Solidworks and printed from a 3D thermal jet printer as one solid piece. The second generation robot also replaced the phase link joint in favor of separate gears for each wing pair. The phase difference between the forewing and hindwing is set by aligning the gears with the proper angular displacement. The driven gear shown in Figure 8(a) has also been replaced by a link, which is lighter and also minimizes the inertial effect due to the angular momentum of the gear. Figure 10(a) shows the modified airframe, and Figure 10(b) shows the assembled second generation prototype.

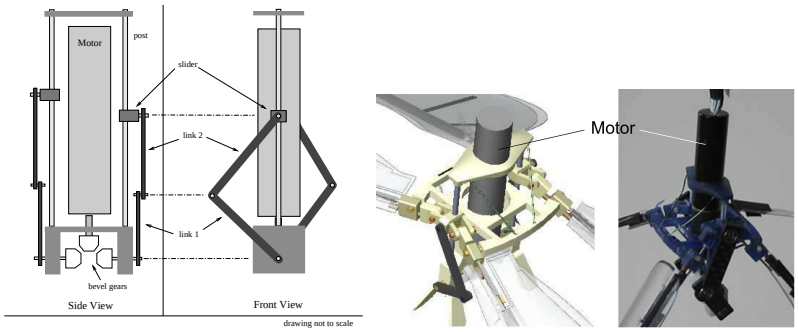


(a) Gear mechanism (second generation) (b) Assembled prototype (second generation)

Figure 10: Gear mechanism and assembled prototype of the second generation robot

The airframe of the second prototype was created utilizing rapid prototyping, which allowed for a complex shape while maintaining a small size. The various working components (pin joints, sliders) were manufactured in the same way. The wing frame was created from carbon fiber beams and covered with a polyester film, .003 inches thick. The completed wing weighed approximately 1.5 grams and was 6.25 inches long. The passive rotation joint was created from carbon fiber beams and tubes, which exhibited a very good stiffness to weight ratio. Lightweight wire was fed through the airframe and top plate to keep the posts (stainless steel rods covered with Teflon tubes) joining the two in constant compression. A Maxon RE 10 motor (capable of 0.75 watts) drives the Delrin miter gears, which in turn drive carbon fiber links attached to the sliders. Figure 11 compares the robotic prototypes from both generations.

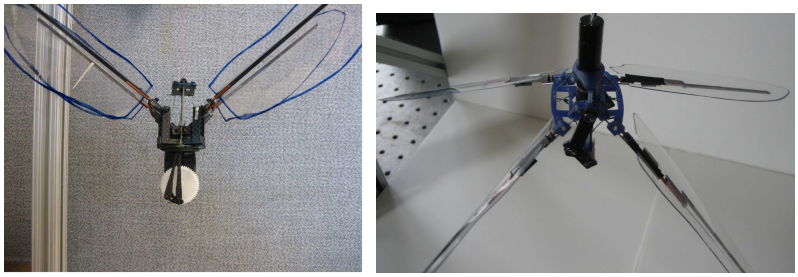

(a) Design overview (first generation) (b) Assembled prototype (second generation)

Figure 11: Full view of robotic prototypes

# 4 Analysis and Experimentation

## 4.1 Wing Kinematics

The analytical forward kinematics of the wing (flapping angles) are calculated as follows:

$$z = r * \cos(\theta) + l * \cos(\sin^{-1}(r/l * \sin(\theta))) \tag{2}$$

$$\phi = tan^{-1}((h - b - z)/a) \tag{3}$$

where $\theta$ is the input angle (gear angle), $\phi$ is the output angle (flapping angle), r is the radius of gear, l is the length of rod linkage, z is the height of slider, a is the horizontal distance from slider pin joint to stationary pin joint, b is the offset on slider, h is the height of stationary pin joint measured from gear centerline, $\Delta$ is the offset distance of wing spar. The definitions of these variables are depicted in Figure 12.

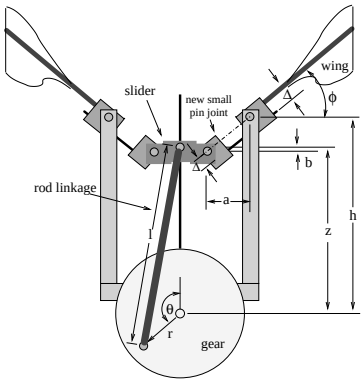


Figure 12: Kinematic Schematic

The actual flapping angle, rotation angle and wing beat frequency were measured using high speed camera as follows. The wing was orientated so that the camera was directed perpendicularly to the stroke plane. A small strip of tape (shown in Fig. 13(a)), 1 inch long, was placed along the chord of the wing. As the rotational angle of the wing changes, the projected length of this strip on the stroke plane changes; From the tape length, the rotational angle $\phi$ can be determined through the following equation, $\phi = \arcsin(l/1)$ where the $l$ is the projected length of the strip (and the denominator, 1, is the actual length of the strip). The flapping angle can be measured

directly from the image, since the stroke plane is paralell with the image. A snapshot of the wings in motion is shown Figure 13(b).

The motion was captured using a high speed Allied Vision Technology CCD Camera at 80 frames per second. The prototype runs up to 8 Hz. Each camera image was saved in National Instrument's Vision Assistant for LabVIEW. A Virtual Instrument (VI) was created to calibrate the pixels to real world units of inches. Each image was then sequentially analyzed in LabVIEW to measure the flapping angle and the length of a the tape strip.

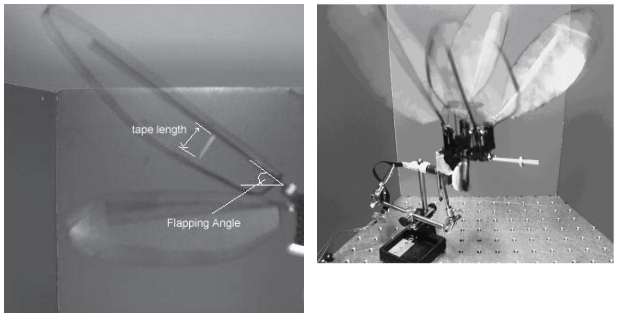


(a) Camera Captured Image (b) Prototype in motion

Figure 13: Experiments to measure wing kinematics

It can be seen in Figure 14(a) that the actual flapping angle of the prototype is very close to the analytical angle derived by assuming perfect mechanism stiffness and constant motor velocity. Since the rotation of the wing is entirely passive, the rotation angle depends on the aerodynamic and inertial forces exerted on it. The measured angle-of-attack are compared to the actual dragonfly kinematics in Figure 14(b). Note that the prototype data is plotted in phase. To smooth out the rotational angle, rotational springs can be mounted on the hindwings to prevent the sharp changes in angles of attack.

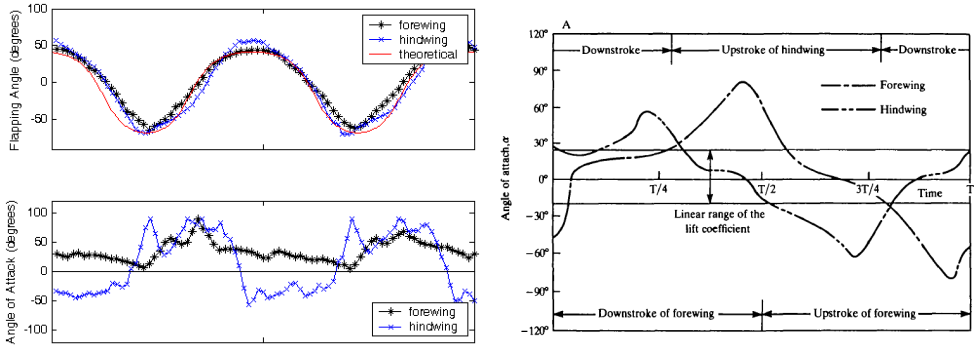


(a) Prototype Flapping Angle and Angle-of-Attack (b) Actual Dragonfly Angle-of-Attack

Figure 14: (a) The measured flapping angle and angle-of-attack for the fore- and hind-wing through two cycles. Black data is for the forewing, blue data for the hindwing. The red line is the theoretical flapping angle assuming a constant motor velocity. (b) Actual dragonfly angles of attack for fore- and hind-wing [5].

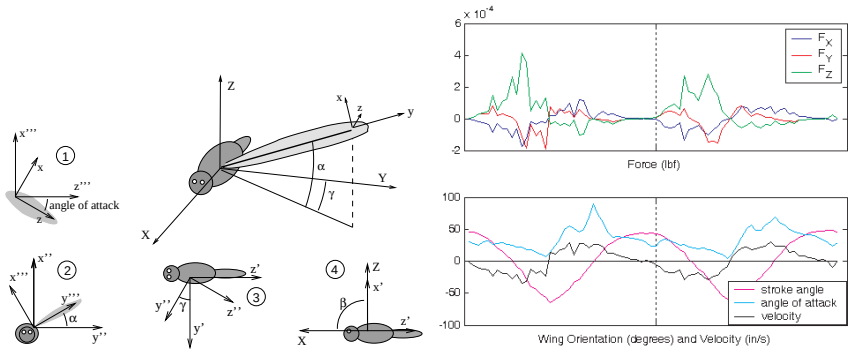


(a) Coordinate frame transformations (b) Analytical aerodynamic forces for forewing

Figure 15: Coordinate Systems and Analytical Aerodynamic Forces.

## 4.2 Aerodynamic Force Generation

### 4.2.1 Aerodynamic Forces Based on Quasi-steady Analytical Model

The aerodynamic forces on the wing were calculated using the kinematic data obtained from experimentation, based a quasi-steady state aerodynamic model:

$$F = C_D * \rho * S * U^2 \tag{4}$$

Where $\rho$ is the air density, S is the wing area and U wing velocity. The drag coefficient ($C_D$) was calculated assuming the wing was a flat plate, and its value were taken from [33]. The wing velocity ($u$) was calculated by mapping a spline to the flapping angle data points (Fig. 14(a)), and then using a midpoint finite difference formula to estimate the velocity between each data point.

This aerodynamic forces were then expressed in the body coordinate frame using the coordinate transformation from wing frame as in 5.

$$F_{body} = Rot(y,\beta) * Rot(x,\gamma) * Rot(z,\alpha) * Rot(y,A) * Trans(c_p,-r,0) * F_{wing} \tag{5}$$

$c_p$ is the distance from the center of pressure of the wing to the wing spar. $r$ is the distance from the center of pressure to the axis of rotation of the wing. All rotational transformations give coordinates expressed in the current frame. $\beta$ and $\alpha$ are defined as in Figure 1. $\gamma$ is the angle the stroke plane makes with the plane of symmetry of the body. $A$ is the angle of attack of the wing. The transformation diagrams are given in Figure 15(a). The aerodynamic forces expressed in the body frame are shown in Figure 15(b). The lift generated ($F_Z$) can be seen to be mainly directed upwards, and periods of negative lift are due to the non-ideal behavior of the wing with respect to its angle of attack.

### 4.2.2 Aerodynamic Forces from Passive Rotation

The wing passive rotation kinematics that are actually generated by the prototype can be reproduced by the flapper, which allows for force measurements and comparison with active rotation. Both experiments utilize the same wing size and Reynolds number.

The active kinematics utilize both a flapping and rotation actuation, shown in Figure 16(a). The passive kinematics use only the flapping signal. The passive rotation of the wing is achieved using a mechanism similar to the passive rotation joint from the prototype, shown in Figure 16(b). The screw is able to rotate in the slot in the base (which attaches to the force sensor). It constrains the wing's rotational position while allowing free rotation within this range. The force sensor coordinate system is also labeled in this figure.

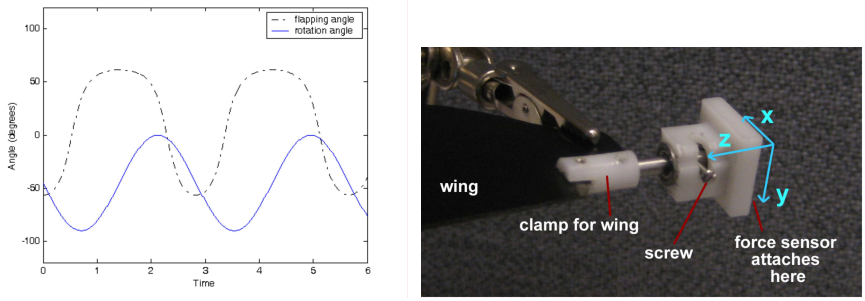


(a) Experimental Kinematics (b) Experimental Passive Rotation Joint

Figure 16: Experimental Setup to Compare Passive and Active Rotation

The actual lift generated by the forces measured in the experiment is determined by transforming the force perpendicular to the surface of the wing, into global coordinates. Figures 17(a) and 17(b) show the total force on the wing (Fy), the lift force components (in the global coordinate system), as well as the average force over a cycle.

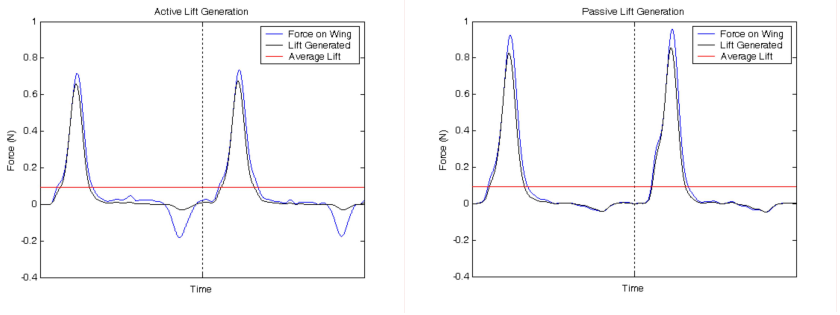


(a) Force generation for active kinematics (b) Force generation for passive kinematics

Figure 17: Force Comparison Between Passive and active rotation

The average lift generated using the active kinematics is 0.0738 Newtons, while the average lift generated for the passive kinematics is 0.0937 Newtons. The passive kinematics actually generate more lift than the active kinematics, despite the simpler mechanism which it would require. This is due to the faster wing rotation during stroke reversal in the passive case.

### 4.2.3 Force Measurements on Prototype

The lift generated by the prototype can be measured directly by the force sensor. The prototype was hung from the sensor by a wire. Two carbon fiber tubes are fixed to the sides of the prototype, and these tubes slide inside

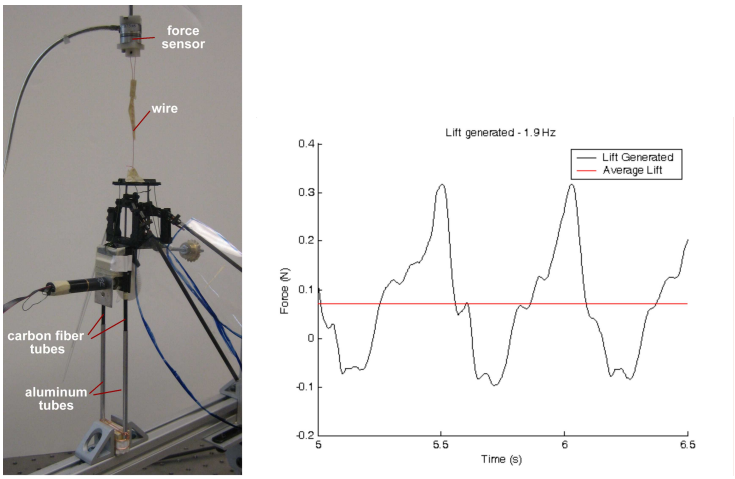


(a) Experimental set-up for measuring lift

(b) Sample lift generation with 1.9Hz frequency

Figure 18: Vertical Force Measurements on Prototype

aluminum tubes which are fixed to the ground. The prototype is able to easily slide up and down, which is required to ensure that the force sensor is exposed to the complete vertical forces on the prototype. The set-up successfully limits the lateral motion of the prototype, shown in Figure 18(a).

The forces generated by the prototype were measured three times, at varying flapping frequencies (1.85Hz, 1.9Hz, and 2.2Hz) over a ten second interval. The data from the force sensor was filtered with a second-order low bypass Butterworth filter. A portion of the resultant data is shown in Figure 18(b) for frequency of 1.9Hz. The average lift increases with flapping frequency. Note that the vertical force includes both aerodynamic and inertial forces.

The average lift generated by the prototype is given in Table 2. This average lift can be used to calculate a sustainable weight it could support. The table also shows the peak vertical force measured.

Table 2: Lift at various frequencies

| Wingbeat Frequency (Hz) | Average Lift (N) | Peak Life (N) | Sustainable Weight (g) |
|---|---|---|---|
| 1.85 | .0342 | 0.18 | 3.48 |
| 1.9 | .0684 | 0.31 | 6.97 |
| 2.2 | .0821 | 0.39 | 8.37 |

# 5 Conclusions and Future Work

This paper presented the design and development of dragonfly-inspired robot. To investigate the aerodynamic forces on dragonfly flight, we have developed a robotic flapper apparatus to measure wing-wing interaction and phase difference effect in dragonfly flight, and to develop design guidelines for the robotic dragonflies. We have

designed two generations of dragonfly robot equipped with two pairs of separate wings driven by DC motors. The phase difference of the forewing and hindwing can be varied by a coupler link in the robot mechanism. To simplify the design, one motor is driving both wings to achieve the desired flapping angle, while angle of attack is achieved through wing passive rotation. Kinematics and aerodynamic forces are calculated analytically and measured on robot experiments.

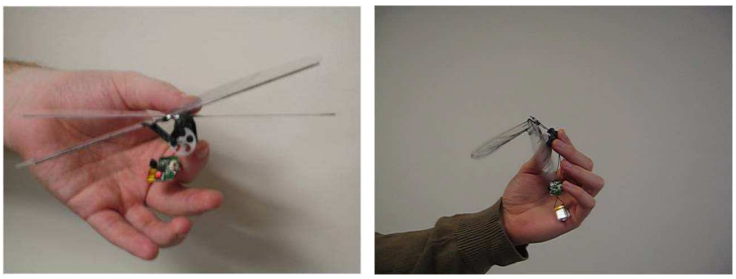

(a) Assembled prototype (third generation) (b) Prototype in motion (third generation)

Figure 19: Third generation prototype: wingbeat frequency up to 10Hz, weight 4 grams including batteries and electronics. For videos of this prototype and previous generation ones, please see http://research.me.udel.edu/deng

On-going and future work include minimizing the size and weight of the robot and increasing the flapping frequency, in order to achieve lift generation which can sustain its weight. Furthermore, adding batteries and electronics on-board while minimizing the weight is also a challenge. Figure 19 shows current prototype we are working on. With one pair of wing, it runs up to 10 Hz and weighs 4 grams total including batteries and electronics. The size and weight is substantially smaller than the previous generations. Nevertheless, to achieve high wingbeat frequency and sufficient lift generation still requires further optimizations of the design. Long term goals of the robot prototype development also include dynamic variable phase difference design during flight.

# 6 Acknowledgement

We would like to thank the Nanorobotics Lab in Carnegie Mellon University for using their thermal jet printer in making the 3D airframe of the second generation robot. This research is supported in part by the NSF award 0545931.

# REFERENCES

[1] D. Alexander, "Unusual phase relationships between the forewing and hindwings in flying dragonflies," *Journal of Experimental Biology*, vol. 109, pp. 379–383, 1984.

[2] R. Norberg, "Hovering flight of the dragonlfy: Aeschna juncea i. kinematics and aerodynamics," *Swimming and Flying in Nature*, vol. 2, pp. 763–780, 1975.

[3] Wowwee, http://www.wowwee.com/en/products/toys/flight/flytech:dragonfly.

[4] Delfly, website: http://www.delfly.nl/.

[5] I. W. Akira Azuma, Soichi Azuma and T. Furuta, "Flight mechanics of a dragonfly," *JEB*, vol. 116, pp. 79–107, 1985.

[6] M. Yamamoto and K. Isogai, "Measurement of unsteady fluid dynamic forces for a mechanical dragonfly model," *AIAA Journal*, vol. 43, no. 12, 2005.

[7] S. P. Sane and M. H. Dickinson, "The aerodynamic effects of wing rotation and a revised quasi-steady model of flapping flight," *Journal of Experimental Biology*, vol. 205, pp. 1087–1096, 2002.

[8] M. Sun and J. H. Wu, "Aerodynamic force generation and power requirements in forward flight in a fruit fly with modeled wing motion," *Journal of Experimental Biology*, vol. 206, pp. 3065–3083, 2003.

[9] S. P. Sane and M. H. Dickinson, "The control of flight force by a flapping wing: Lift and drag production," *Journal of Experimental Biology*, vol. 204, pp. 2607–2626, 2001.

[10] R. B. S. R. L. N. Adrian L.R. Thomas, Graham K. Taylor and R. J. Bomphrey, "Dragonfly flight: Free-flight and tethered flow visualizations reveal a diverse array of unsteady lift-generating mechanisms, controlled primarily *via* angle of attack," *Journal of Experimental Biology*, vol. 207, pp. 4299–4323, 2004.

[11] J. Wakeling and C. Ellington, "Dragonfly flight I. gliding flight and steady-state aerodynamic forces," *Journal of Experimental Biology*, vol. 200, pp. 543–556, 1997.

[12] ——, "Dragonfly flight II. velocities, accelerations and kinematics of flapping flight," *Journal of Experimental Biology*, vol. 200, pp. 557–582, 1997.

[13] ——, "Dragonfly flight III. lift and power requirements," *Journal of Experimental Biology*, vol. 200, pp. 583–600, 1997.

[14] A. B. Kesel, "Aerodynamic characteristics of dragonfly wing sections compared with technical aerofoils," *Journal of Experimental Biology*, vol. 203, pp. 3125–3135, 2000.

[15] Z. J. Wang, "The role of drag in insect hovering," *Journal of Experimental Biology*, vol. 207, pp. 4147–4155, 2004.

[16] J. M. Birch and M. H. Dickinson, "The influence on wing-wake interations on the production of aerodynamic forces in flapping flight," *Journal of Experimental Biology*, vol. 206, pp. 2257–2272, 2003.

[17] S. P. Sane, "Review: The aerodynamics of insect flight," *Journal of Experimental Biology*, vol. 206, pp. 4191–4208, 2003.

[18] M. Sato and A. Azuma, "The flight performance of a damselfly *Ceriagrion Melanurum* Selys," *Journal of Experimental Biology*, vol. 200, pp. 1765–1779, 1997.

[19] R. J. Bomphrey, N. J. Lawson, N. J. Harding, G. K. Taylor, and A. L. R. Thomas, "The aerodynamics of manduca sexta digital partical image velocimetry analysis of the leading-edge vortex," *Journal of Experimental Biology*, vol. 208, pp. 1079–1094, 2005.

[20] A. P. Willmont and C. P. Ellington, "the mechanics of flight in the hawkmoth *Manduca Sexta*," *Journal of Experimental Biology*, vol. 200, pp. 2705–2722, 1997.

[21] R. B. Srygley and J. G. Kingsolver, "Effects of weight loading on flight performance and survival of palatable Neotropical *Anartia fatima* butterflies," *Biological Journal of the Linnean Society*, vol. 70, pp. 707–725, 2000.

[22] K. Y. Masato Okamoto and A. Azuma, "Aerodynamic characteristics of the wings and body of a dragonfly," *Journal of Experimental Biology*, vol. 199, pp. 281–294, 1996.

[23] J. Wang and M. Sun, "A computational study of the aerodynamics and forewing-hinwing interaction of a model dragonfly in forward flight," *Journal of Experimental Biology*, vol. 208, pp. 3785–3804, 2005.

[24] A. C. Neville, "Aspects of flight mechanics in anisopterous dragonflies," *Journal of Experimental Biology*, vol. 37, pp. 631–656, 1960.

[25] L. F. Dickinson, M. H. and S. P. Sane, "Wing rotation and the aerodynamic basis of insect flight," *Science*, vol. 284, pp. 1954–1960, June 1999.

[26] J. M. B. Z. Jane Wang and M. H. Dickinson, "Unsteady forces and flows in low Reynolds number hovering flight: Two-dimensional computations *vs* robotic wing experiments," *Journal of Experimental Biology*, vol. 207, pp. 449–460, 2004.

[27] Z. J. Wang, "Dissecting insect flight," *Annual Review of Fluid Mechanics*, vol. 37, pp. 183–210, 2005.

[28] C. Ellington, "The aerodynamics of hovering insect flight. iii. kinematics," *Phil. Trans. R. Soc. Lond. B*, vol. 305, pp. 41–78, 1984.

[29] R. A. Norberg, "The pterostigma of insect wings an inertial regulator of wing pitch," *J. Comp. Physiol.*, vol. 81, pp. 9–22, 1972.

[30] M. M. Winson Lai, Joseph Yan and S. Green, "Force measurements on a scaled mechanical model of dragonfly in forward flight," in *International Conference on Advanced Robotics*, 2005, pp. 595–600.

[31] W. J. Maybury and F.-O. Lehmann, "The fluid dynamics of flight control by kinematic phase lag variation between two robotic insect wings," *Journal of Experimental Biology*, vol. 207, pp. 4707–4726, 2004.

[32] C. DiLeo, "Development of a tandem-wing flapping micro aerial vehicle prototype and experimental mechanism," Master's thesis, University of Delaware, 2007.

[33] M. H. Dickinson, F. O. Lehmann, and S. S. Sane, "Wing rotation and the aerodynamic basis of insect flight," *Science*, vol. 284, no. 5422, pp. 1954–1960, 1999.